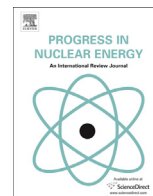




Contents lists available at ScienceDirect

Progress in Nuclear Energy

journal homepage: www.elsevier.com/locate/pnucene

Monte Carlo and nodal neutron physics calculations of the IAEA MTR benchmark using Serpent/DYN3D code system



Marat Margulis, Erez Gilad*

The Unit of Nuclear Engineering, Ben-Gurion University of the Negev, Beer Sheva 84105, Israel

ARTICLE INFO

Article history:

Received 19 August 2015

Received in revised form

1 December 2015

Accepted 21 December 2015

Available online 9 January 2016

Keywords:

Serpent

DYN3D

Monte Carlo

Reactor physics

Burnup

Research reactor

ABSTRACT

As part of recent efforts to utilize NPPs computational methodologies to safety analysis of research reactors, the Serpent and DYN3D codes were extensively compared with a variety of static and burnup calculations as defined in the IAEA benchmark for 10 MW MTR pool-type reactor. These calculations include unit cell calculations and few group constants generation, unit cell and full core k -eigenvalue and burnup calculations, and full core 3D flux and power distributions. The Serpent code capabilities as a lattice code for MTR plate-type fuel assemblies were evaluated and compared with EPRI-CELL and WIMS-D4 results and reference solutions for full 3D core models were compared with MCNP5 and OpenMC results. The DYN3D nodal diffusion code capabilities in modeling full 3D MTR cores were also evaluated using few group cross sections and assembly discontinuity factors obtained by Serpent unit cell calculations. The DYN3D results were compared with Serpent, MCNP5 and OpenMC.

© 2016 Elsevier Ltd. All rights reserved.

1. Introduction

Research Reactors (RRs) are developed and built primarily as test facilities and neutron generators for vast range of scientific, industrial and medical purposes. Unlike commercial nuclear power plants (NPPs), RRs are characterized by small core size, low total thermal power, high power density, low fuel and clad temperatures and low system pressure. Furthermore, the different fuel composition, geometric configuration and different ranges of relevant operational parameters constitute different neutronic and thermal-hydraulics designs (D'Auria and Bousbia-Salah, 2006; Adorni et al., 2006, 2007; Hamidouche et al., 2008). As a result, these reactors must meet different safety requirements and unique safety features to ensure their safe utilization in nominal and off-nominal operation conditions and safe shutdown in case of an emergency or an accident. Moreover, many research reactors are characterized by constantly changing operational environment, e.g. irradiation of new materials and fuels, introduction of new instrumentation into the core, different core loading configurations, varying irradiation regimes and so on. Hence, the

reactor safety analysis report is frequently updated and must include the analysis of a wide variety of safety related scenarios. Furthermore, the uniqueness of each RR and its experimental systems make the standardization of design, operation and licensing of RRs a non-trivial task (Hamidouche et al., 2008; Costa et al., 2011).

The safety analysis methodology employed for existing NPPs is based on a well-established and very active international community of experts, well founded and proven methods and computational tools including best-estimate codes and uncertainty analysis, international standardization and extensive and accessible experimental database (D'Auria et al., 2006; Bousbia-Salah and D'Auria, 2007). During the last decade, the IAEA and others (Hamidouche et al., 2004; D'Auria and Bousbia-Salah, 2006; IAEA, 2007; Costa et al., 2011) have acknowledged the importance of implementing the well-founded and mature NPP safety technology (methods, codes, regulations and guidelines) in RRs safety analysis methodology and reassess their safety features (Adorni et al., 2007).

However, the characteristics of RRs are different from those for NPP, due to different geometries and design, fuel compositions, structural materials and thermal-hydraulic operation regime (Hamidouche et al., 2004; D'Auria and Bousbia-Salah, 2006; Chatzidakis et al., 2014). The adequacy of applying NPP computational

* Corresponding author.

E-mail address: gilade@bgu.ac.il (E. Gilad).

tools to RRs has been addressed in several thermal-hydraulic transients studies using RELAP5 (Woodruff et al., 1996, 1997; Bretscher et al., 1999; Deen et al., 1999; Hari et al., 2000; Adorni et al., 2005, 2006, 2007; Hedayat et al., 2007; Lu et al., 2009; Azzoune et al., 2010; Hamidouche and Bousbia-Salah, 2010; Omar et al., 2010; Reis et al., 2010; Chatzidakis et al., 2014; Khan et al., 2014; Soares et al., 2014; Abdelrazek et al., 2015), PARET (Deen et al., 1999; Housiadas, 2000; Chatzidakis et al., 2012, 2014), ATHLET (Hainoun and Schaffrath, 2001), coupled NK/TH PARCS/RELAP5 (Hamidouche et al., 2009), and COBRA-EN (Arshi et al., 2015). Recently, few studies solved the IAEA 10 MW MTR benchmark for the purpose of validating advanced neutronic codes and data libraries, e.g. MCNP5 (Bousbia-Salah et al., 2008) and OpenMC (Chaudri and Mirza, 2015).

The vast majority of the studies mentioned above utilize the IAEA benchmark for 10 MW Material Test Reactor (MTR) pool-type reactor for assessing their codes performances (IAEA, 1980). The benchmark was specified under the program of research reactor core conversion from highly enriched uranium (HEU) to low enrichment uranium (LEU) cores. The benchmark consists of detailed steady state neutronic and thermal-hydraulic calculations and a range of different accident and transient scenarios (IAEA, 1992). However, recent years show a growing trend of benchmarking codes against actual experimental measurements for code evaluation (Chatzidakis et al., 2013, 2014), which became publicly available. Such experimental data was collected and compiled during the IAEA CRP 1496 activity between 2008 and 2013 (IAEA, 2008, 2010, 2011, 2012, 2015) and other international efforts (Chatzidakis et al., 2013, 2014; Hainoun et al., 2014), and includes static measurements as well as neutronic and thermal-hydraulic transient data.

The main goal of this article is to evaluate the Serpent Monte Carlo code (Leppanen, 2007; Leppanen et al., 2015) capabilities as a lattice code for MTR plate-type fuel assemblies and the DYN3D nodal diffusion code (Grundmann et al., 2000, 2005) capabilities in modeling full MTR cores. The calculation scheme utilizes the Serpent code for unit cell and burnup calculations, including few group cross sections and assembly discontinuity factors generation, as well as for reference full core calculations. The obtained few group constants are then used by the nodal code DYN3D for full 3D core benchmark. Once the DYN3D utilization for static MTR reactor calculation is completed and verified, the ultimate goal is to use it for transient analysis in research reactors. The DYN3D has the capability to solve the time dependent neutron diffusion equation for full 3D core couple to thermal-hydraulic channel code, but it has not yet been employed for studying transients in research reactors.

The current study consists of three-dimensional Monte Carlo (MC) and deterministic nodal diffusion calculations, which are compared with the results in (IAEA, 1980) and with EPRI-CELL, WIMSD4, MCNP5 and OpenMC codes (Bousbia-Salah et al., 2008; Chaudri and Mirza, 2015). For this purpose the latest version of Serpent and DYN3D codes were used. This article reports on the first stage in the development of a transient thermal-hydraulic system code for research reactor accidents analysis – THERMO-T, which eventually will interface with the core model of DYN3D via the core inlets and outlets and use its three-dimensional nodal diffusion code (Margulis and Gilad, 2015). THERMO-T is currently undergoing comprehensive comparisons to different codes in different accident scenarios available in the IAEA TECDOC 643 (IAEA, 1992) and the IAEA Technical Reports Series No. 480 (IAEA, 2015), which provide both numerical (code-to-code) and experimental data for reactivity insertion and loss of flow accidents for different types of reactors.

2. Methodology

2.1. Serpent

Serpent is a continuous energy Monte Carlo neutron transport code with burnup capabilities developed at VTT research center in Finland (Leppanen, 2007; Leppanen et al., 2015). This code allows modeling of complicated three-dimensional geometries, and was developed as an alternative to deterministic lattice codes for generation of homogenized multigroup constants for reactor analyses using nodal codes. The current version of Serpent contains libraries based on JEFF-2.2, JEFF-3.1.1, ENDF/B-VI.8 and ENDF/B-VII evaluated data files. In this work the ENDF/B-VII evaluated data files were used.

The Serpent code has a number of features that dramatically reduces CPU time required for its execution, among them are a unified energy grid for storing cross section data and the use of Woodcock delta-tracking of particles. Serpent also has a built-in subroutine for fuel depletion that is based on the CRAM method (Pusa, 2013). All nuclides and meta-stable states data contained in the decay libraries are available for Serpent calculations, where the total number of different nuclides produced from fission, transmutation and decay reactions is in the order of 1500. The atom densities of all included nuclides with decay data are tracked in the burnup calculation, and the number of nuclides with cross sections typically ranges from 200 to 300.

The depletion analysis can be performed with a predictor-corrector (PC) algorithm to get a more accurate estimate of isotopic concentrations at each time step. In Serpent, there are two ways of tallying 1-g cross sections. The most accurate way is tallying directly each type of reaction rate for each isotope in each burnable material. In this study Serpent is used to generate few group cross sections and assembly discontinuity factors as well as for reference full core calculations.

2.2. DYN3D

The code DYN3D (Grundmann et al., 2000, 2005) is a three-dimensional coupled neutron kinetics and thermal-hydraulics core code, developed at Helmholtz-Zentrum Dresden-Russendorf (HZDR) for dynamic and depletion calculations in light water reactor cores with rectangular or hexagonal lattice geometry. The multigroup neutron diffusion equation is solved by nodal methods coupled to a thermal-hydraulic model (FLOCAL). The core is modeled by parallel coolant channels which can describe one or more fuel elements. Starting from the critical state (critical boron concentration or critical power), the code allows to simulate the neutronic and thermal-hydraulic core response to reactivity changes and/or changes of the coolant core inlet conditions. Cross section libraries generated by different lattice codes for different reactor types are linked with DYN3D. Although DYN3D was developed for analyzing power reactors and was intensively validated and verified against power reactors benchmarks, it is shown in this study that DYN3D is also suitable for studying research reactors, such as the one considered in this work.

2.3. Core description

In the current work both HEU and LEU cores were modeled. The core grid consists of 6×7 grid, containing 21 fuel elements, 4 control elements, and graphite and water reflectors. The geometry and dimensions of a standard fuel element is presented in Fig. 1. Each standard fuel element consists of 23 fuel plates, whereas the control fuel elements contain 17 fuel plates, as shown in Fig. 2. The core configuration for both Beginning of Life (BOL) and End of Life

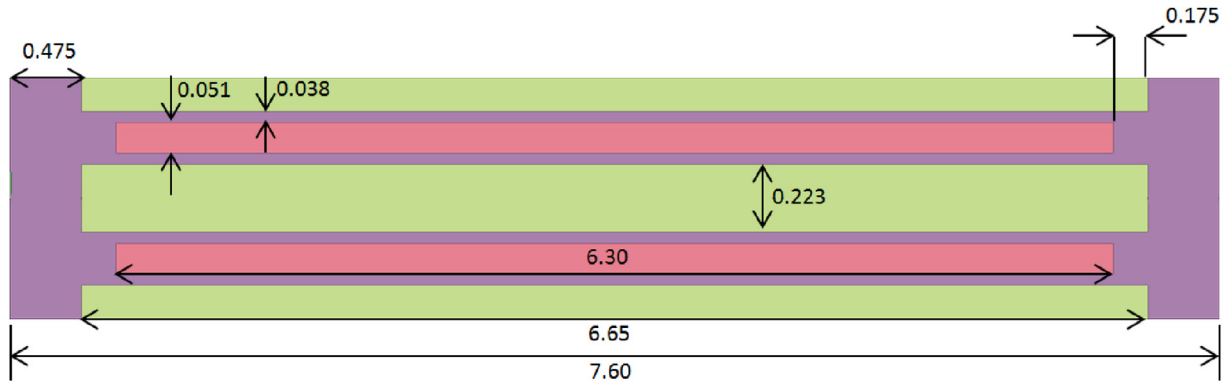


Fig. 1. Geometry and dimensions of a standard MTR fuel element. Dimensions are in cm.

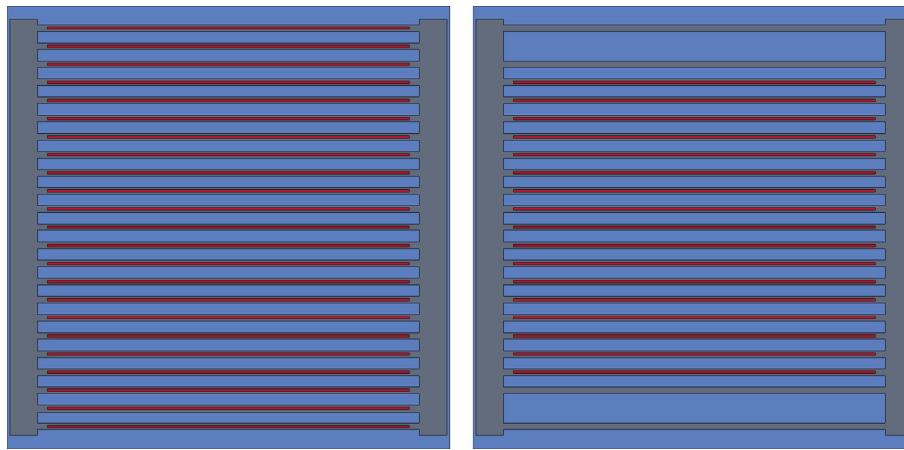


Fig. 2. Mid-plane XY cross section of a standard (left) and control (right) fuel elements as modeled in Serpent.

(EOL), as a function of ^{235}U depletion is shown in Fig. 3. The core is surrounded by graphite and water reflectors. The active core height of 60 cm is followed on both sides by 15 cm of axial Al–H₂O

reflectors containing volume fractions of 20% Al and 80% water and by additional 15 cm of water. A summary of the benchmark specifications is given in Table 1.

water	graphite	graphite	graphite	graphite	water
water	Fuel BOL 5% EOL 10%	Fuel BOL 25% EOL 30%	Fuel BOL 25% EOL 30%	Fuel BOL 5% EOL 10%	water
Fuel BOL 5% EOL 10%	Control BOL 25% EOL 30%	Fuel BOL 45% EOL 50%	Fuel BOL 45% EOL 50%	Control BOL 25% EOL 30%	Fuel BOL 5% EOL 10%
Fuel BOL 25% EOL 30%	Fuel BOL 45% EOL 50%	Fuel BOL 45% EOL 50%	water	Fuel BOL 45% EOL 50%	Fuel BOL 45% EOL 50%
Fuel BOL 5% EOL 10%	Control BOL 25% EOL 30%	Fuel BOL 45% EOL 50%	Fuel BOL 45% EOL 50%	Control BOL 25% EOL 30%	Fuel BOL 5% EOL 10%
water	Fuel BOL 5% EOL 10%	Fuel BOL 25% EOL 30%	Fuel BOL 25% EOL 30%	Fuel BOL 5% EOL 10%	water
water	graphite	graphite	graphite	graphite	water

Fig. 3. MTR core configuration for both Beginning of Life (BOL) and End of Life (EOL) as a function of ^{235}U depletion.

Table 1
Summary of the MTR core and fuel assemblies benchmark specifications.

Benchmark Parameters (IAEA, 1980)	
Active core height	600 mm
Space at the grid plate per fuel element	77 × 81 mm
Fuel element	76 × 80.5 mm (with support plate) 76 × 80.0 mm (without support plate)
Meat dimensions	63 × 0.51 × 600 mm
Density of Aluminum-clad	2.7 g/cm ³
Support plate (Aluminum):	
- Thickness	4.75 mm
- Density	2.7 g/cm ³
Fuel plate:	
- Thickness	1.27 mm
- # per fuel element	23
- # per control element	17
Remaining plate positions of the control element:	
4 aluminum plates ($\rho_{Al} = 2.7 \text{ g/cm}^3$), each 1.27 mm thick in the position of the 1st, 3rd, 21st, and 23rd standard plate positions; Water gaps between the two sets of aluminum plates.	
Graphite element:	
- Dimensions	77 × 81 mm
- Density	1.7 g/cm ³
UAl _x -Al fuel:	
- HEU	Enrichment 93 wt.% ²³⁵ U 280 g ²³⁵ U per fuel element
- LEU	21 wt.% of uranium in the UAl _x -Al Enrichment 20 wt.% ²³⁵ U 390 g ²³⁵ U per fuel element
	72 wt.% of uranium in the UAl _x -Al
Total power	10 MW _{th}
Thermal-hydraulic conditions:	
- Water temperature	20° C
- Fuel temperature	20° C
- Pressure at core height	1.7 bar

2.4. Calculation methodology

The Serpent code allows a free meshing in order to obtain flux tally more accurately. In the current case, three energy groups were considered (E_n denotes the neutron energy): a **fast group**, where $E_n > 5.531$ keV, an **epithermal group**, where $0.625 \text{ eV} < E_n < 5.531 \text{ keV}$, and a **thermal group**, where $E_n < 0.625 \text{ keV}$. Six different core configurations were considered, i.e. HEU and LEU cores for fresh, BOL, and EOL configurations. In the BOL and EOL configuration, each fuel element has different ²³⁵U depletion according to the benchmark specifications, as shown in Fig. 3. In the fresh core configuration, all fuel elements are fresh. The Serpent calculations were performed with 20 inactive cycles followed by 200 active cycles, each consisting of 150,000 histories, and the source neutrons were randomly distributed on each fuel plate. In order to ensure the convergence of the Serpent simulations and the minimization of the statistical uncertainty, the Shannon entropy method was used as a measure of the fission source distribution convergence (Brown, 2006; Fridman and Leppanen, 2012). This option is embedded in the Serpent code and was invoked throughout the calculations. Radial and axial cross sections of the Serpent three-dimensional full core model are shown in Fig. 4.

The Monte Carlo Serpent calculations were used also to generate few group cross sections and assembly discontinuity factors (ADFs) to be used by DYN3D for full core calculations. For this purpose, two energy groups were selected, with 0.625 eV as the boundary between them. In recent years it was noticed by the Serpent users community that the neutron balance is not preserved in nodal codes when using few group constants which were generated by Serpent (Fridman and Leppanen, 2012). In recent Serpent versions, some problems related to multiplication effects of (n, xn) reactions were fixed, thus improving the accuracy of the few group constants

in fuel elements (Fridman and Leppanen, 2012). However, while the few group constants generation procedure for fuel elements was clarified, the treatment of ADFs for non-fuel elements, e.g. reflectors, remained untouched. In order to calculate fuel ADFs, a single fuel assembly was considered with reflective boundary conditions. Then, the Serpent's built-in module for ADF calculation was invoked via the card – “set adf 1”. Invoking this card provides the user with the heterogeneous and homogeneous surface fluxes and currents, as well as the calculated ADFs by solving Eq. (1) and Eq. (2) in the fuel region. As an example, the few group constants and ADFs for the BOL HEU core are summarized in Table 2. The up-scattering interaction is neglected.

In order to overcome this inaccuracy problem, a special procedure was implemented outside Serpent for the ADFs generation for reflector regions (Fridman et al., 2013). First, a one-dimensional fuel-reflector heterogeneous flux problem, as schematically described in Fig. 5a, is solved by Serpent to obtain the homogeneous few group constants for the reflector area. In addition, the fuel-reflector interface fluxes ϕ_s^{het} and currents J_s are calculated for further estimation of reflector ADFs. Second, the one-dimensional few group homogeneous diffusion equation (1) is solved for the reflector region, with J_s as a boundary condition as schematically described in Fig. 5b, in order to obtain the homogeneous flux:

$$-D_g \frac{d^2 \phi_g}{dx^2} + \sum_{t,g} \phi_g = \sum_{g'=1}^G \sum_s \phi_{g'} \quad (1)$$

where D is the diffusion coefficient, Σ_t is the total cross section, Σ_s is the scattering cross section, G is the total number of energy groups and g indicates the energy group. The reflector discontinuity factor (DF) is then calculated as the ratio between heterogeneous and homogeneous interface fluxes:

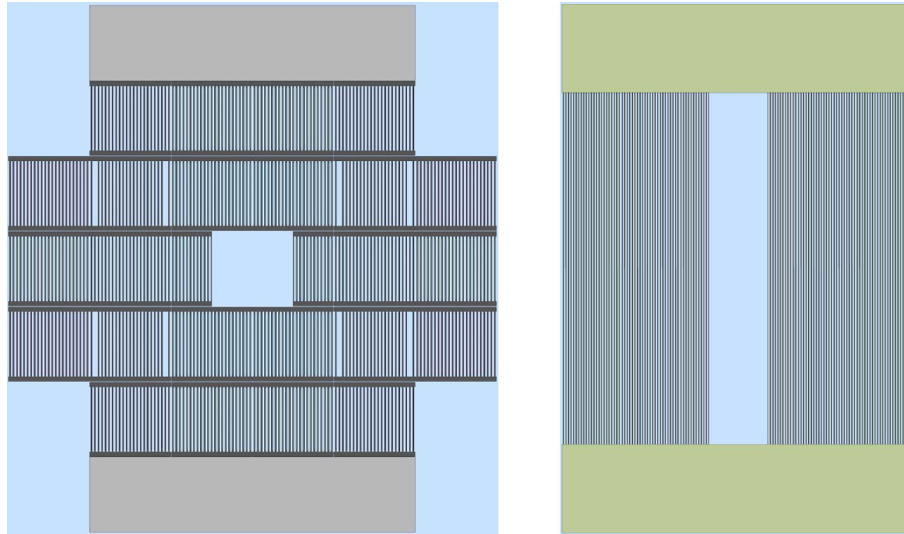


Fig. 4. Radial XY (left) and axial XZ (right) cross sections of the Serpent three-dimensional full core model of the IAEA 10 MW MTR benchmark.

Table 2
Example for the macroscopic cross sections and ADFs for the BOL HEU core.

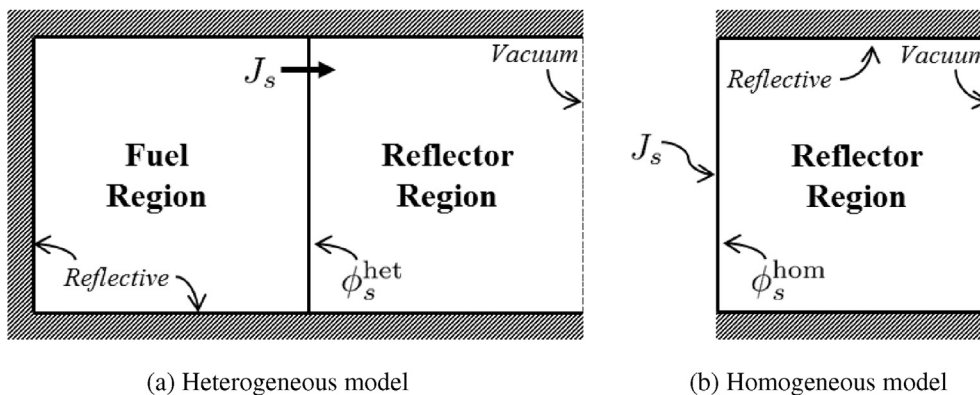
	Energy Group	Fuel 5% BU	Fuel 25% BU	Fuel 45% BU	Top axial Reflector	North radial Reflector
$\Sigma_{tr,g}$	1	0.2039	0.2042	0.2049	0.1564	0.2544
	2	1.1100	1.1308	1.2480	1.7160	0.2963
$\Sigma_{a,g}$	1	0.0032	0.0030	0.0023	0.0004	0.0000
	2	0.0932	0.0810	0.0616	0.0174	0.0002
$\nu\Sigma_{f,g}$	1	0.0043	0.0034	0.0026	0.0000	0.0000
	2	0.1571	0.1299	0.0907	0.0000	0.0000
$\Sigma_{s,gg'}$	1 → 1	0.5473	0.5482	0.5655	0.6594	0.3209
	2 → 1	0.0000	0.0000	0.0000	0.0000	0.0000
	1 → 2	0.0264	0.0266	0.0284	0.0473	0.0025
DF_{west}	2 → 2	1.6300	1.6586	1.8300	2.4960	0.4193
	1	0.9846	0.9859	0.9931	1.0000	1.0000
DF_{north}	2	1.0230	1.0180	1.0050	1.0000	1.0000
	1	1.0140	1.0180	1.0320	1.0000	1.0000
DF_{east}	2	1.0080	0.9773	1.0170	1.0000	1.0000
	1	0.9846	0.9859	0.9931	1.0000	1.0000
DF_{south}	2	1.0230	1.0180	1.0050	1.0000	1.0000
	1	1.0140	1.0180	1.0320	1.0000	0.9830
DF_{bottom}	2	1.0080	0.9773	1.0170	1.0000	0.9738
	1	1.0000	1.0000	1.0000	1.1150	1.0000
DF_{top}	2	1.0000	1.0000	1.0000	0.8056	1.0000
	1	1.0000	1.0000	1.0000	1.0000	1.0000
	2	1.0000	1.0000	1.0000	1.0000	1.0000

$$DF_g = \frac{\phi_{s,g}^{het}}{\phi_{s,g}^{hom}} \quad (2)$$

3. Burnup calculations

The burnup capabilities of Serpent were studied using the effective unit cell (IAEA, 1980) shown in Fig. 6 and compared to the benchmark results by Argon National Laboratory (ANL) EPRI-CELL (IAEA, 1980) and WIMS-D4 (Bousbia-Salah et al., 2008). The burnup calculations results, as well as the relative errors between the different codes, for HEU and LEU fuel are shown in Figs. 7 and 8, respectively. The numbers are summarized in Tables A.1 and A.2, respectively. The corresponding infinite multiplication factors k_∞ and differences between the different codes are shown in Fig. 10 for both HEU and LEU cases. The numbers are summarized in Table B.1. The burnup calculations were carried out with constant power of 302.5 W/cm, assuming total core power is 10 MW, the number of fuel plates is $21 \times 23 + 4 \times 17 = 551$, and active core height of 60 cm.

The atom densities, calculated by Serpent, of ^{238}U show



(a) Heterogeneous model

(b) Homogeneous model

Fig. 5. A typical super-assembly geometry for one-dimensional fuel-reflector model.

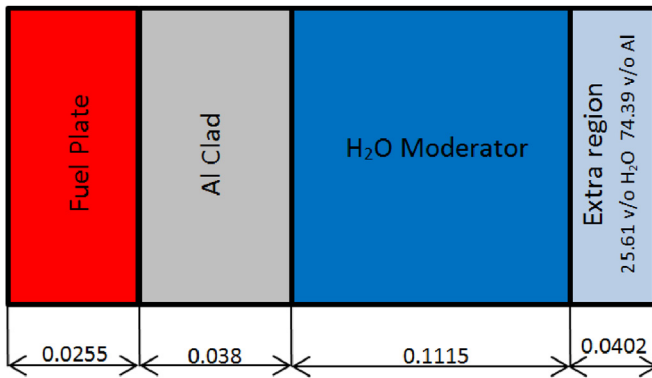


Fig. 6. The effective unit cell used for benchmark burnup calculation by ANL (IAEA, 1980) and WIMS-4D (Bousbia-Salah et al., 2008).

excellent agreement with both EPRI-CELL and WIMS-D4 calculated densities for both HEU and LEU fuel, with an average relative error¹ of less than 0.1%. The ²³⁶U atom densities also show very good agreement with an average relative error of 0.2% and 1.5% with respect to the EPRI-CELL and WIMS-D4 results, respectively. The ²³⁹Pu atom densities calculated by Serpent for the HEU case are smaller than those calculated by EPRI-CELL (WIMS-D4) by 16.9% (12.3%) at 5% depletion, and reduces monotonically to 7.4% (5.4%) at 50% depletion. In the LEU case however, the initial error (at 5% depletion) is 6.3% (5.8%) and then fluctuates around 1% (2%) up to 50% depletion. These differences originate from differences in neutron data libraries (e.g. ENDF/B-IV and WIMS libraries used by EPRI-CELL and WIMS-D4 codes, respectively), especially in the ²³⁸U (*n,γ*) cross section data, and from the resonance shielding and resonance integrals calculations. While the calculation of these physical quantities is straight forward in Serpent, deterministic lattice codes utilize a variety of approximations to evaluate these quantities. Moreover, the relatively large errors are also due to the small amount of ²³⁹Pu, especially in the HEU case.

Since in the LEU case more ²³⁵U is present in the core with respect to the HEU case, the neutron spectrum is slightly harder, as calculated by Serpent and shown in Fig. 9. Hence, the ²³⁸U resonance absorption in the epithermal energies is more dominant in the LEU case with respect to the HEU case. This fact, together with the larger initial amount of ²³⁸U in the core, leads to higher ²³⁹Pu production in the LEU case with respect to the HEU case. According to Serpent results, the number of ²³⁹Pu nuclei present in the core constitutes 6–10% of the number of ²³⁵U nuclei depleted in the LEU case, but less than 0.5% in the HEU. Furthermore, the number of ²³⁸U nuclei depleted in the core constitutes 12–14% of the number of ²³⁵U nuclei depleted in the LEU case, but only 0.6% in the HEU. It should also be noted that these errors are comparable to the errors between the EPRI-CELL and WIMS-D4 results, and that large errors in ²³⁹Pu atom densities also exist between the different participants in the original benchmark.

Regarding poisonous fission products, there exist significant differences between EPRI-CELL and WIMS-D4 calculated atom densities of ¹³⁵Xe and ¹⁴⁹Sm. The relative error between EPRI-CELL and WIMS-D4 for ¹³⁵Xe atom densities is rather constant and fluctuates around 6.0% (4.8%) for HEU (LEU) case. The Serpent results show very good agreement with WIMS-D4 calculations, with

an average relative error of 0.1% (0.5%) for HEU (LEU) case. However, the average relative error between EPRI-CELL and WIMS-D4 for ¹⁴⁹Sm atom densities is significantly larger. The initial error is approximately 5% (at 5% depletion) which monotonically increases to approximately 60% at 50% depletion for both HEU and LEU cases, whereas the EPRI-CELL code consistently underestimates the ¹⁴⁹Sm amount with respect to WIMS-D4. These large errors (in %) are due to very small atom densities values. Interestingly, the Serpent results for ¹⁴⁹Sm atom densities mostly indicate intermediate values between the EPRI-CELL and WIMS-D4 results, i.e. Serpent results overestimate the ¹⁴⁹Sm amount with respect to EPRI-CELL results but underestimate it with respect to WIMS-D4 results. Serpent results for ¹⁴⁹Sm deviate initially by approximately 2% (7%) from the EPRI-CELL (WIMS-D4) results, and increases monotonically up to 30% (20%) at 50% depletion for both HEU and LEU cases. This inconsistency is most likely the result of differences in fission yield values, decay constants, and decay chains accounted for in the burnup schemes of the different codes. In addition, despite the same power level, the softer spectrum in the HEU case (see Fig. 9) results in a lower ¹³⁵Xe and ¹⁴⁹Sm densities with respect to the LEU case.

In recent years Monte Carlo burnup calculations are becoming much more affordable for fuel cycle analyses of existing and future nuclear reactors. These calculations are characterized by coupling of a Monte Carlo eigenvalue and flux solver and a fuel depletion module (Pusa, 2013). The neutron flux distribution and the isotopes microscopic cross sections are calculated by the Monte Carlo solver and transmitted to the fuel depletion module. To the best of our knowledge, the burnup calculations performed by Serpent in this study are the first available results of this benchmark which were calculated using a Monte Carlo burnup code without coupling to other external deterministic codes. For example, both (Bousbia-Salah et al., 2008) and (Chaudri and Mirza, 2015) use the WIMS-D4 code for burnup calculations, where the calculated atom densities are then fed into MCNP5 or OpenMC.

The unit cell k_{∞} calculations are compared in Fig. 10 for both HEU and LEU cases. In the HEU case, the initial difference between EPRI-CELL and WIMS-D4 is 50 pcm (at 0% depletion) and increases up to 150 pcm at 50% depletion. The Serpent results are consistently higher, with an initial difference of 390 (440) pcm at 0% depletion with respect to EPRI-CELL (WIMS-D4) results, and increasing up to 480 (630) pcm at 50% depletion. In the LEU case, the differences between EPRI-CELL and WIMS-D4 results range between 40 and 150 pcm, whereas the Serpent results are again consistently higher, with differences range between 190 and 280 (270–370) pcm with respect to EPRI-CELL (WIMS-D4) results.

In addition, a comparison of the Serpent generated few group cross section was performed against the ANL benchmark results. The comparison includes fission and absorption cross sections for ²³⁵U and ²³⁸U, where the absorption cross section was calculated as the sum of fission and capture cross sections, neglecting the other non-dominant reactions. Reflective boundary conditions were used and no effective buckling was assigned nor other reflector saving approximations. This comparison is necessary since this study includes the full core modeling of the MTR reactor core in DYN3D code. The results are summarized Tables 3 and 4 for HEU and LEU fuel, respectively.

The few group absorption (σ_a) and fission (σ_f) microscopic cross sections for ²³⁵U show very good agreement between Serpent and EPRI-CELL, with an average deviation in absorption of 2.7%, –1.1%, and –3.2% for the fast, epithermal, and epithermal groups, respectively, and 1.5%, 0.4%, and –3.3% in fission few group cross sections, for both HEU and LEU cases. The absorption cross section of ²³⁸U also show very good agreement between Serpent and EPRI-CELL, with an average deviation of 0.9%, 2.7%, and –2.3% for the

¹ The relative error (between two values N_A and N_B) is defined according to $e = (N_A - N_B)/N_A$ in percentage. The relative error is calculated for each burnup level, $e \equiv e(BU)$ and the “average relative error” is the average over the relative errors for different burnup levels, i.e. $\bar{e} = \frac{1}{N_{BU}} \sum_{i=1}^{N_{BU}} e(BU_i)$, where $BU_i = 0\%, 5\%, 10\%, \dots$

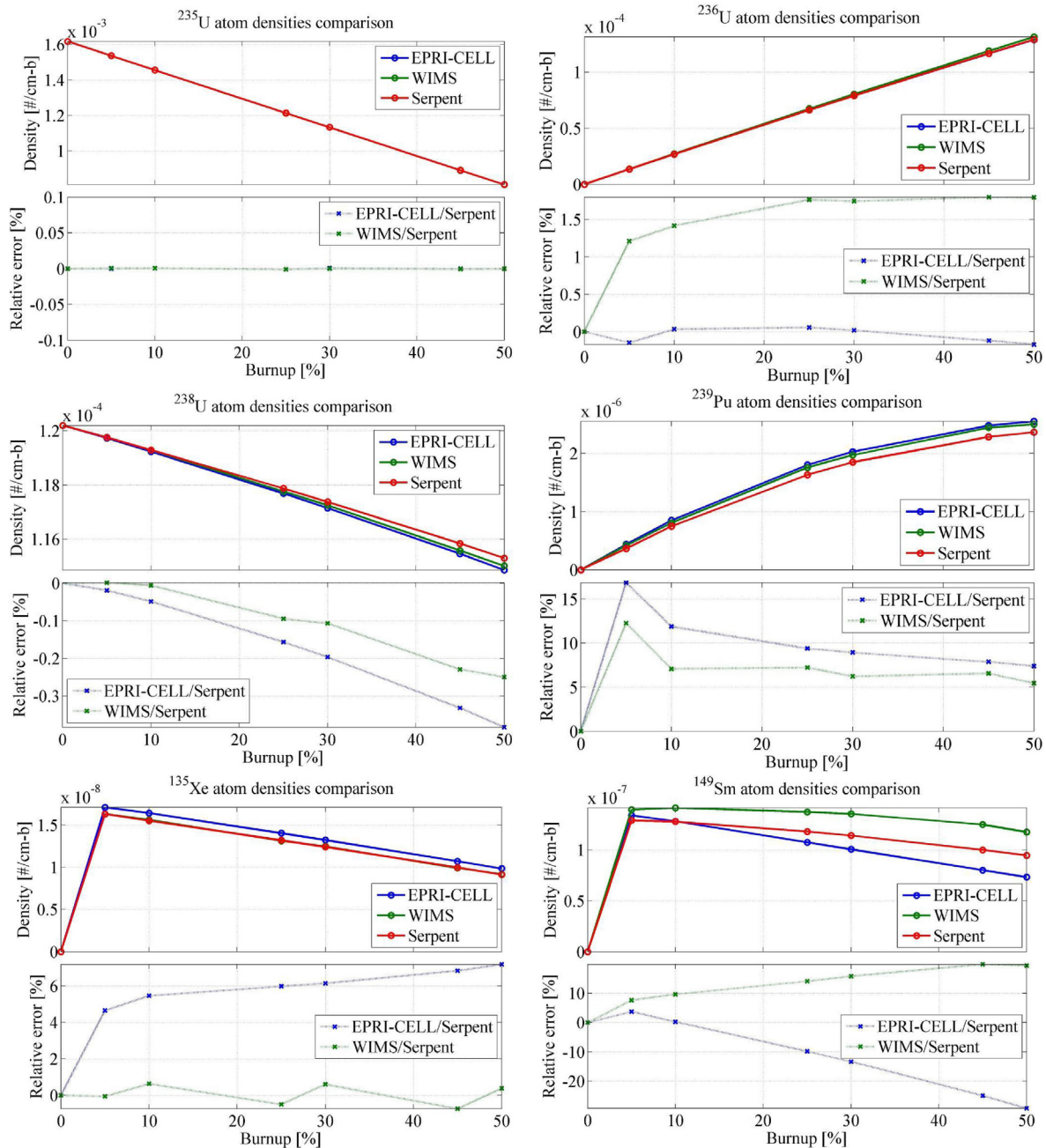


Fig. 7. Atom densities for HEU fuel vs. burnup – comparison and relative errors between ANL EPRI-CELL (IAEA, 1980), WIMS-D4 (Bousbia-Salah et al., 2008) and Serpent.

HEU case and 0.9%, -4.6% , and -3.1% for the LEU case, as well as the fission cross sections of ^{238}U for the fast group with an average deviation of -2.0% for both HEU and LEU. However, The fission cross section of ^{238}U calculated by Serpent for the epithermal group is significantly larger than the one calculated by EPRI-CELL code for both HEU and LEU (by a factor of ~ 3.5). Remaining plate positions of the to originate from pronounced differences in neutron data libraries used by EPRI-CELL code (ENDF/B-IV) and Serpent (ENDF/B-VII.1).

4. Full core calculations

4.1. k_{eff} calculations

The effective multiplication factor k_{eff} of the different benchmark cases, calculated by both Serpent and DYN3D using 2-groups cross sections and ADFs generated by Serpent, are compared with MCNP5 and OpenMC results in Table 5. As can be seen from Table 5, the results vary depending on the codes and neutron data libraries. However, the results of both Serpent and DYN3D are in an excellent agreement with one another, and in very good agreement with MCNP5 and OpenMC results.

The distinct effect of the usage of ADFs in full core calculations is demonstrated in Table 5. The differences in k_{eff} values between

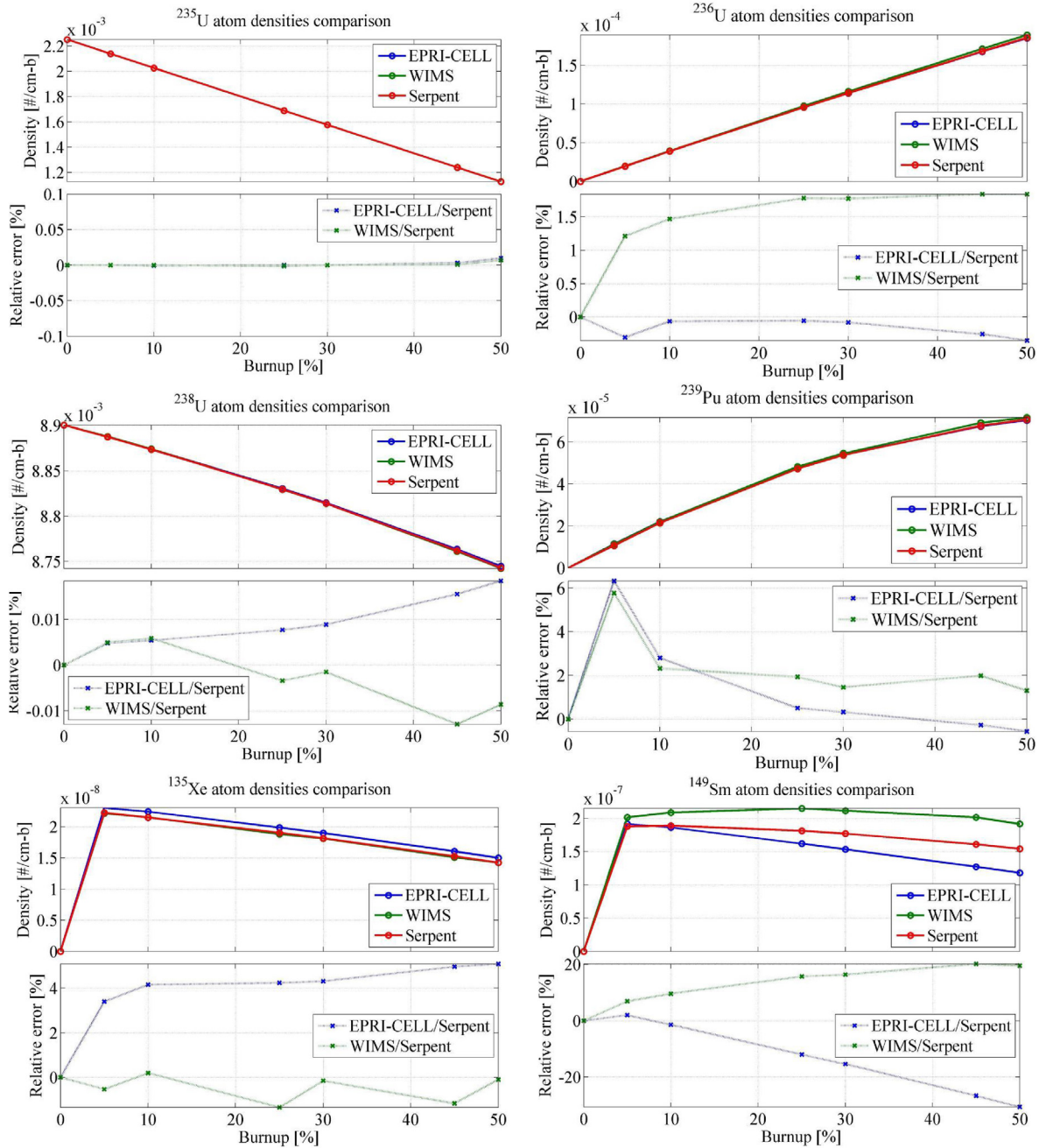


Fig. 8. Atom densities for LEU fuel vs. burnup – comparison and relative errors between ANL EPRI-CELL (IAEA, 1980), WIMS-D4 (Bousbia-Salah et al., 2008) and Serpent.

DYN3D and Serpent (diff row) drop from 50 to 150 pcm to less than 30 pcm once ADFs are used in the calculation by DYN3D, for all the cores considered. These ADFs were calculated according to section 2.4.

4.2. Flux distribution

Serpent allows plotting of two-dimensional meshes, indicating the thermal flux and fission power distributions in the core, as shown in Fig. 11 for the HEU core at BOL. The cold and hot shades represent relative thermal flux and relative fission rate (power) distributions, respectively. Bright and dark colors indicate high and low values, respectively. The mid-plane radial flux distribution and the axial flux distribution in the flux trap of the HEU BOL core is

shown in Fig. 12 using three energy groups.

In MCNP5 the neutron flux is calculated in terms of neutron flux per source neutron, hence the absolute flux value is obtained via multiplication by the number of source neutrons. However, in Serpent the flux is normalized by the mesh volume. Therefore, the mesh was spread according to the benchmark specifications, i.e. a total of 51 mesh intervals in the x-direction and 56 in the y-direction from the center of the XY plane. Furthermore, all the diffusion codes utilized in the benchmark used reflector savings on one end of 8 cm. However, in MCNP5 (Bousbia-Salah et al., 2008), OpenMC (Chaudri and Mirza, 2015) and Serpent, the model includes a 15 cm Al-H₂O reflector followed by additional 15 cm of water on both sides in the axial direction.

The core average flux axial distribution in three energy groups

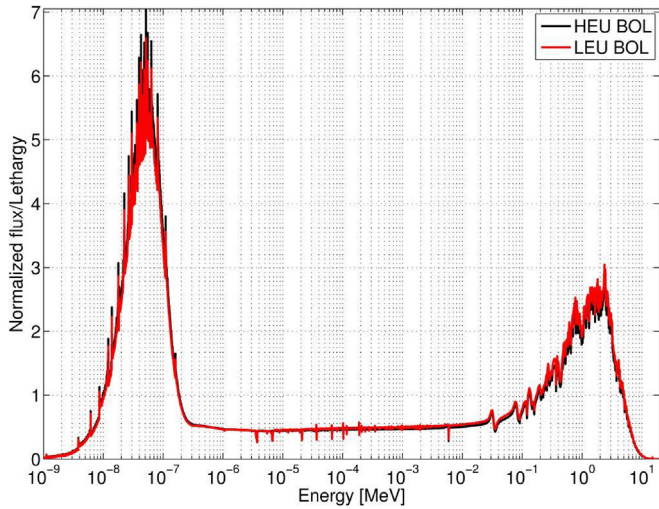


Fig. 9. The neutron flux energy spectrum of HEU and LEU cores at BOL calculated by Serpent.

for both HEU and LEU cores at BOL and EOL is shown in Fig. 13. The axial flux distributions are very similar to a cosine shape, except in the fuel-reflector interface, where a small rise in the thermal flux is evident. The thermal flux axial distribution in the flux trap is shown in Fig. 14.

4.3. Power distribution

Normalized power distributions calculated by Serpent for both HEU and LEU at BOL and EOL are shown in Fig. 15. As expected, the results are highly symmetric and show good agreement with the results obtained with MCNP5 (Bousbia-Salah et al., 2008) and OpenMC (Chaudri and Mirza, 2015). The relative errors (in %) of the normalized power distribution calculated by OpenMC and MCNP5 with respect to Serpent, per each fuel element, are shown in Fig. 16. The same power distributions were also calculated by DYN3D using the few group constants (cross sections and discontinuity factors) obtained by Serpent unit cell calculations. The relative errors (in %) of the normalized power distribution calculated by DYN3D with respect to Serpent, per each fuel element, are shown in are shown

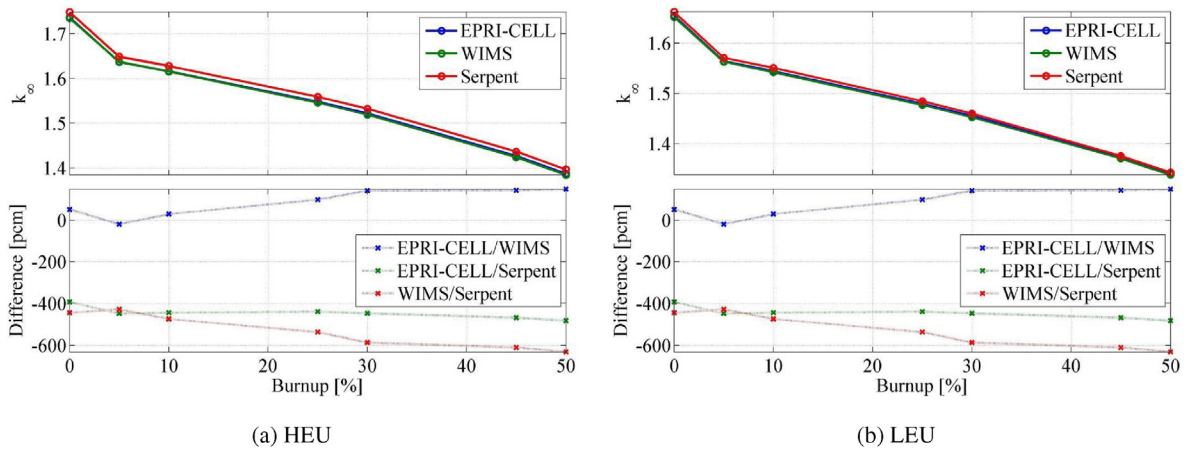


Fig. 10. Unit cell infinite multiplication factor k_{∞} for HEU and LEU fuel vs. burnup – comparison between ANL EPRI-CELL (IAEA, 1980), WIMS-D4 (Bousbia-Salah et al., 2008) and Serpent.

Table 3 Serpent cross sections vs. burnup for HEU fuel compared to ANL EPRI-CELL code (IAEA, 1980).

Depletion (%)	Energy group	²³⁵ U				²³⁸ U			
		EPRI-CELL		Serpent		EPRI-CELL		Serpent	
		σ_a	σ_f	σ_a	σ_f	σ_a	σ_f	σ_a	σ_f
0	1	1.72709	1.45346	1.68029	1.43138	0.34526	0.17997	0.34205	0.18377
	2	39.2357	25.9938	39.6335	25.8309	27.1369	6.18E-5	26.3254	2.25E-4
	3	422.841	360.532	435.815	371.815	1.76920	0	1.81598	0
5	1	1.72712	1.45348	1.68090	1.43174	0.34526	0.17997	0.34220	0.18351
	2	39.3375	26.0492	39.7325	25.8836	27.1610	6.17E-5	26.3386	2.26E-4
	3	422.092	359.877	432.852	369.259	1.76614	0	1.80495	0
10	1	1.72714	1.45350	1.68041	1.43148	0.34527	0.17997	0.34201	0.18376
	2	39.4375	26.1024	39.8757	25.9668	27.1873	6.17E-5	26.5196	2.43E-4
	3	426.152	363.376	439.400	374.873	1.78135	0	1.82879	0
25	1	1.72723	1.45355	1.68090	1.43172	0.34529	0.17997	0.34218	0.18346
	2	39.7422	26.2640	40.1153	26.0964	27.2681	6.15E-5	26.6439	2.40E-4
	3	439.696	375.049	452.151	385.806	1.83197	0	1.87508	0
30	1	1.72726	1.45357	1.68122	1.43196	0.34530	0.17997	0.34242	0.18369
	2	39.8452	26.3188	40.2093	26.1520	27.2962	6.15E-5	26.6039	2.40E-4
	3	444.598	379.273	456.550	389.581	1.85028	0	1.89114	0
45	1	1.72734	1.45362	1.68151	1.43213	0.34532	0.17997	0.34218	0.18338
	2	40.1578	26.4871	40.5022	26.3274	27.3855	6.15E-5	26.6439	2.43E-4
	3	460.633	393.090	472.050	402.857	1.91013	0	1.94728	0
50	1	1.72737	1.45364	1.68178	1.43225	0.34533	0.17998	0.34174	0.18322
	2	40.2632	26.5449	40.6415	26.4011	27.4174	6.13E-5	26.6069	2.35E-4
	3	466.486	398.133	477.843	407.820	1.93195	0	1.96833	0

Table 4
Serpent cross sections vs. burnup for LEU compared to ANL EPRI-CELL code (IAEA, 1980).

Burnup (%)	Energy group	²³⁵ U				²³⁸ U			
		EPRI-CELL		Serpent		EPRI-CELL		Serpent	
		σ_a	σ_f	σ_a	σ_f	σ_a	σ_f	σ_a	σ_f
0	1	1.72920	1.45441	1.68354	1.43301	0.34362	0.17851	0.34039	0.18188
	2	37.8447	25.2009	38.3385	25.1447	6.09503	6.38E-5	6.36171	2.22E-4
	3	392.606	334.476	407.323	347.369	1.65603	0	1.71211	0
5	1	1.72923	1.45443	1.68370	1.43315	0.34363	0.17851	0.34046	0.18196
	2	37.9599	25.2617	38.4627	25.2189	6.10113	6.38E-5	6.36761	2.21E-4
	3	391.023	333.106	406.202	346.389	1.64984	0	1.70782	0
10	1	1.72927	1.45445	1.68353	1.43304	0.34364	0.17851	0.34042	0.18208
	2	38.0696	25.3164	38.5767	25.2752	6.10816	6.37E-5	6.38280	2.31E-4
	3	394.540	336.114	409.687	349.386	1.66310	0	1.72067	0
25	1	1.72937	1.45452	1.68327	1.43287	0.34368	0.17853	0.34059	0.18209
	2	38.3941	25.4691	38.8451	25.4170	6.13249	6.36E-5	6.40733	2.12E-4
	3	406.711	346.645	421.104	359.191	1.70884	0	1.76245	0
30	1	1.72940	1.45454	1.68324	1.43292	0.34369	0.17854	1.98155	0.18232
	2	38.5044	25.5196	38.9533	25.4595	6.14153	6.36E-5	6.43415	2.08E-4
	3	411.253	350.562	425.381	362.864	1.72586	0	1.77808	0
45	1	1.72950	1.45461	1.68366	1.43319	0.34373	0.17856	0.34100	0.18235
	2	38.8488	25.6786	39.2590	25.6158	6.17125	6.35E-5	6.46507	2.12E-4
	3	426.484	363.692	439.960	375.371	1.78287	0	1.83119	0
50	1	1.72953	1.45463	1.68351	1.43310	0.34375	0.17856	0.34076	0.18245
	2	38.9683	25.7349	39.3232	25.6220	6.18209	6.34E-5	6.47100	2.11E-4
	3	432.191	368.610	445.683	380.277	1.80409	0	1.85198	0

Table 5
Comparison of k_{eff} values, calculated by different codes, of the different cases defined in the benchmark (IAEA, 1980).

Organization (code)	HEU (93 wt.%)			LEU (20 wt.%)		
	Fresh	BOL	EOL	Fresh	BOL	EOL
BGU (Serpent) ^a	1.18310	1.02392	1.00037	1.16636	1.02003	1.00074
BGU (DYN3D without ADFs)	1.18391	1.02500	1.00128	1.16707	1.02157	1.00127
diff ^b	58 pcm	102 pcm	90 pcm	52 pcm	147 pcm	57 pcm
BGU (DYN3D with ADFs)	1.18333	1.02421	1.00038	1.16667	1.02000	1.00049
diff ^c	16 pcm	27 pcm	1 pcm	21 pcm	3 pcm	25 pcm
UPisa (MCNP5) ^{d,e}	1.18962	N/A	N/A	1.17238	N/A	N/A
PIEAS (OpenMC) ^{d,e}	1.19382	N/A	N/A	1.15494	N/A	N/A

^a The statistical uncertainty is less than 27 pcm for all simulations.
^b Difference between Serpent and DYN3D without ADFs for axial and radial reflectors.
^c Difference between Serpent and DYN3D with ADFs for axial and radial reflectors.
^d HEU/LEU calculations are available with xenon-free conditions (Bousbia-Salah et al., 2008; Chaudri and Mirza, 2015).
^e The statistical uncertainty is less than 25 pcm.

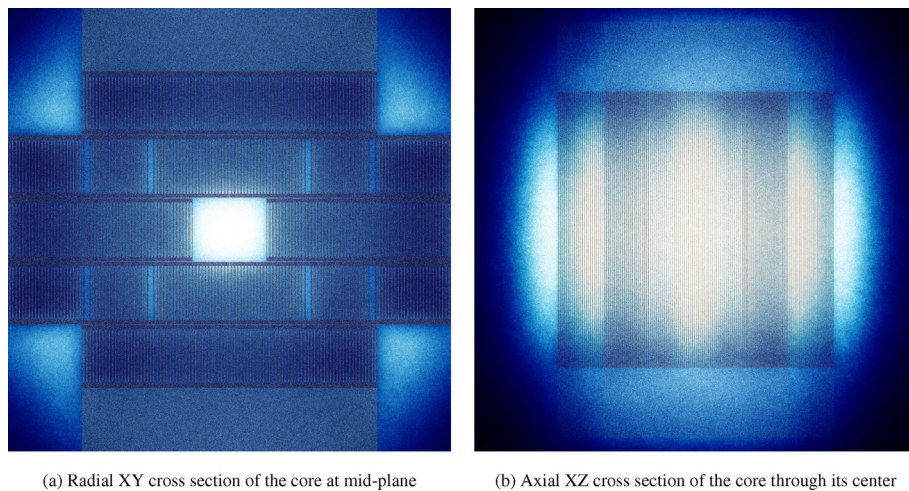


Fig. 11. Serpent two-dimensional mesh plots indicating the thermal flux and fission power distributions in the HEU core at BOL. Cold and hot shades represent relative thermal flux and relative fission rate (power) distributions, respectively. Bright and dark colors indicate high and low values, respectively (For interpretation of the references to colour in this figure legend, the reader is referred to the web version of this article.).

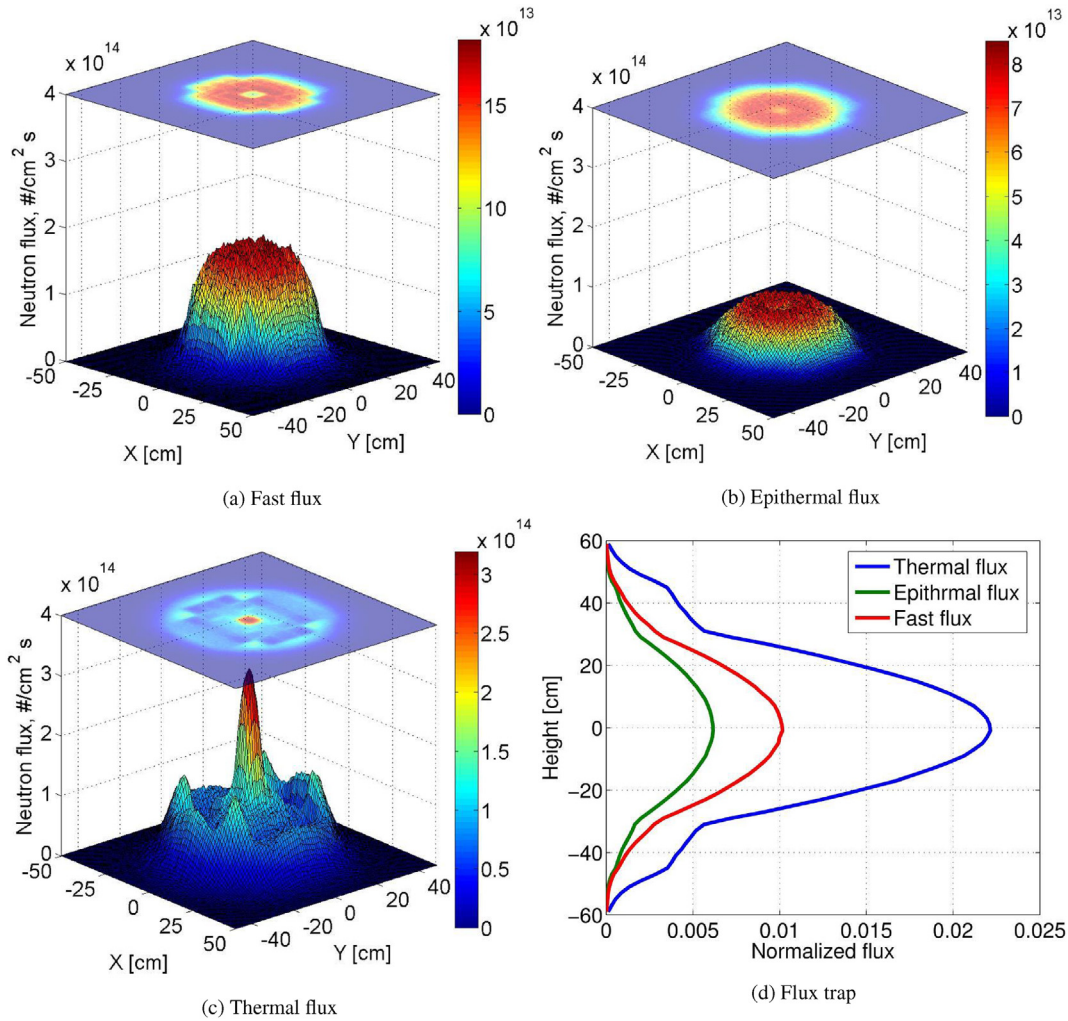


Fig. 12. Serpent calculation of the mid-plane radial flux distribution and the axial flux distribution in the flux trap of the HEU BOL core using three energy groups.

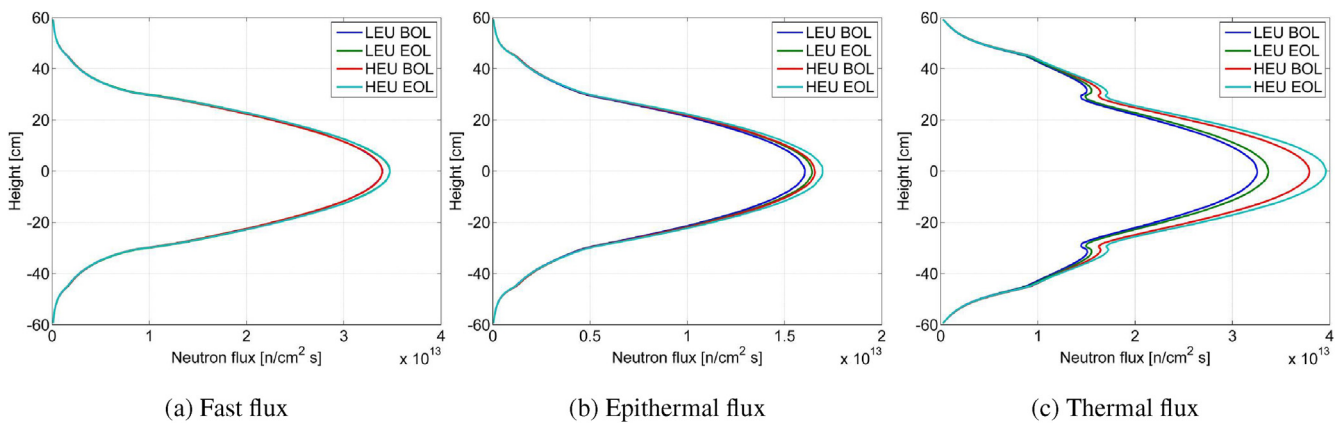


Fig. 13. Serpent calculation of the total flux axial distributions in three energy groups of the HEU and LEU cores at BOL and EOL.

in Fig. 17.

It is clear that OpenMC over-estimates the power in the central fuel elements by 1–3% with respect to Serpent, and under-estimates the power in the peripheral fuel elements by 1–3%. Hence, the power distributions calculated by OpenMC for all cases exhibit higher peaking factors with respect to Serpent. The same

trend is evident also in MCNP5 results, except for the two half-assemblies adjacent to the central flux trap, whose power is under-estimated with MCNP5 by 1–4% with respect to Serpent. Hence, the power peaking factors of the MCNP5 distributions are even higher than the ones of OpenMC.

In contrast to the Monte Carlo codes, the nodal diffusion code

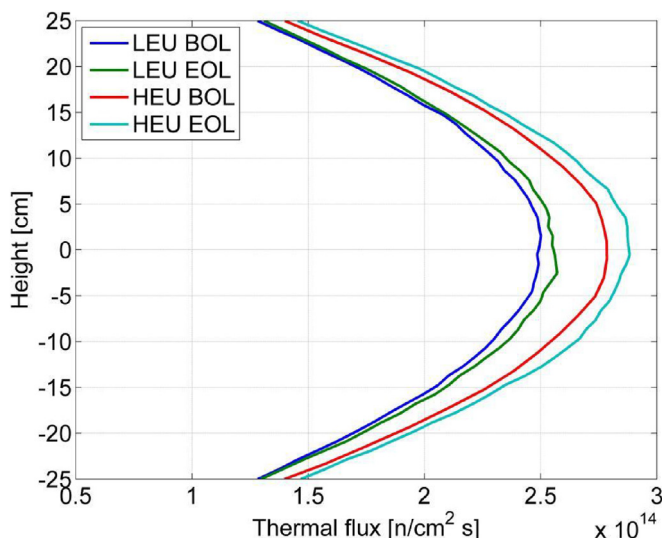


Fig. 14. Serpent calculation of the thermal flux axial distributions in the flux trap.

DYN3D under-estimates the power in the central fuel elements by 2–3% with respect to Serpent, and over-estimates the power in the peripheral fuel elements by 2–4%. Hence, the power distributions calculated by DYN3D for all cases exhibit lower peaking factors with respect to Serpent. This is due to the fact that DYN3D solves the neutron diffusion equation, and despite the sophisticated nodal methods, various transport corrections and the use of ADFs, diffusion approximation still tends to smooth the flux shape with respect to neutron transport calculations. The larger relative errors between DYN3D and Serpent occur in the four corner fuel elements and are due to the 1D nature of the ADFs derivation, which might be insufficient for these corner fuel elements. A 2D ADFs derivation procedure should reduce this deviation. It should be noted that the asymmetry present in Fig. 17 is due to Serpent, since DYN3D results are completely symmetric.

5. Conclusions

The Serpent and DYN3D codes were extensively compared with EPRI-CELL, WIMS-D4, MCNP5 and OpenMC codes in a variety of calculations as defined in the IAEA benchmark for 10 MW MTR pool-type reactor (IAEA, 1980). These calculations include both HEU and LEU fuel compositions, unit cell calculations and few group constants generation, unit cell and full core *k*-eigenvalues and burnup calculations, and full core 3D flux and power distributions.

The Serpent code (Leppanen, 2007; Leppanen et al., 2015) capabilities as a lattice code for MTR plate-type fuel assemblies were evaluated and reference solutions for full 3D core models of HEU and LEU at BOL and EOL were calculated. These calculations were compared with MCNP5 and OpenMC results for *k*_{eff}, flux and power distributions. The DYN3D nodal diffusion code (Grundmann et al., 2000, 2005) capabilities in modeling full 3D MTR cores were also evaluated using few group cross sections and assembly discontinuity factors obtained by Serpent unit cell calculations. The DYN3D results were compared with Serpent, MCNP5 and OpenMC full core calculations for *k*_{eff}, flux and power distributions.

The atom densities, calculated by Serpent, of uranium isotopes ²³⁸U and ²³⁵U show excellent agreement with both EPRI-CELL and WIMS-D4 calculated densities for both HEU and LEU fuel. The differences in ²³⁹Pu densities result from differences in neutron data libraries and approximated resonance shielding and resonance integrals calculations used by deterministic lattice codes. The Serpent results for ¹³⁵Xe atom densities show very good agreement with EPRI-CELL and WIMS-D4 calculations for both HEU and LEU, whereas significant differences exist in ¹⁴⁹Sm densities between the different codes. The Serpent results for ¹⁴⁹Sm densities indicate intermediate values between the EPRI-CELL and WIMS-D4 results. This inconsistency is most likely the result of differences in fission yield values, decay constants, and decay chains accounted for in the burnup schemes of the different codes. To the best of our knowledge, the burnup calculations performed by Serpent in this study are the first available results of this benchmark which were calculated using a Monte Carlo code without coupling to other

water	graphite	graphite	graphite	graphite	water	
	4.21±0.015	3.89±0.011	3.89±0.012	4.22±0.014		
water	4.27±0.014	3.90±0.012	3.90±0.012	4.26±0.020	water	
	4.26±0.006	3.97±0.011	3.97±0.011	4.26±0.018		
	4.31±0.014	3.98±0.012	3.98±0.012	4.32±0.013		
4.04±0.011	3.29±0.013	4.52±0.012	4.52±0.012	3.31±0.012	4.06±0.011	LEU BOL LEU EOL HEU BOL HEU EOL
4.10±0.014	3.31±0.014	4.45±0.014	4.44±0.011	3.31±0.013	4.09±0.014	
4.05±0.012	3.35±0.012	4.43±0.003	4.44±0.003	3.34±0.012	4.05±0.012	
4.11±0.014	3.32±0.019	4.36±0.013	4.36±0.015	3.32±0.013	4.10±0.014	
3.46±0.020	3.75±0.015	2.81±0.014	water	2.81±0.015	3.76±0.010	3.47±0.013
3.47±0.010	3.70±0.016	2.76±0.013		2.76±0.013	3.72±0.012	3.47±0.010
3.42±0.012	3.76±0.012	2.67±0.010		2.67±0.010	3.75±0.012	3.42±0.012
3.50±0.010	3.69±0.014	2.61±0.013		2.60±0.018	3.68±0.012	3.50±0.010
4.05±0.014	3.30±0.017	4.51±0.014		4.52±0.012	3.31±0.012	4.06±0.011
4.09±0.012	3.31±0.013	4.45±0.011		4.46±0.012	3.32±0.013	4.11±0.014
4.06±0.009	3.35±0.012	4.42±0.003		4.43±0.019	3.34±0.012	4.05±0.009
4.10±0.014	3.32±0.019	4.35±0.021		4.36±0.015	3.32±0.013	4.10±0.014
water	4.21±0.015	3.89±0.015	3.90±0.013	4.23±0.011	water	
	4.27±0.014	3.90±0.013	3.91±0.013	4.27±0.013		
	4.26±0.006	3.97±0.004	3.96±0.004	4.27±0.006		
	4.31±0.014	3.97±0.015	3.97±0.012	4.32±0.017		
Water	graphite	graphite	graphite	graphite	water	

Fig. 15. Normalized power distribution calculated by Serpent.

water	graphite	graphite	graphite	graphite	water
	0.40	-0.78	-0.21	-2.64	
water	-1.29	0.17	-0.65	-2.21	water
	-2.26	-0.82	-0.02	-0.80	
	-0.82	0.14	1.70	-0.03	
-0.77	1.45	2.43	1.94	-0.58	-2.35
-2.86	0.54	1.14	2.18	3.83	-2.50
-1.39	0.57	1.28	2.24	-0.29	-1.54
-1.42	-1.08	2.91	1.39	-0.41	2.02
0.86	1.22	1.84	2.70	1.19	-1.51
-0.38	-0.17	2.71	1.12	1.71	-1.91
0.46	1.32	2.54	water	1.15	1.81
0.02	0.97	2.18		2.84	2.09
-0.23	0.96	1.06	0.86	-0.76	-2.35
-1.94	0.99	2.06	2.01	-0.79	-1.27
-2.66	-0.28	3.01	2.56	2.26	-3.37
-1.35	-2.07	1.81	1.32	-0.08	0.29
water	-0.41	-0.34	1.17	-1.61	water
	0.07	0.61	1.50	-1.88	
	-1.73	0.72	-0.75	-0.99	
	-2.93	0.78	-0.86	-2.83	
water	graphite	graphite	graphite	graphite	water

(a) OpenMC (Chaudri and Mirza, 2015)

water	graphite	graphite	graphite	graphite	water
	-2.49	0.79	-0.59	-1.49	
water	-2.41	0.77	1.31	-1.39	water
	-0.36	1.58	0.61	-2.89	
	-1.44	0.48	-1.36	5.07	
-2.75	-0.04	3.84	2.63	1.29	-2.28
-3.37	-1.49	3.89	4.82	0.23	-2.30
-3.53	1.37	2.87	1.55	-0.11	-2.65
-4.99	2.37	1.12	1.03	-1.69	-5.25
-2.49	1.70	-1.93	water	-2.33	4.49
-0.67	5.05	-0.74		-2.22	4.00
0.78	3.83	-1.21	water	-2.67	2.58
-1.52	5.80	-4.18		-3.67	0.08
-4.74	0.02	4.15	4.85	0.84	-1.97
-4.45	0.90	3.62	2.42	-1.00	-3.87
-2.98	-0.40	3.97	3.54	1.13	-3.96
-4.00	0.38	2.51	1.61	0.23	-1.11
water	-1.76	0.13	2.43	-1.77	water
	-2.83	0.74	0.82	-3.19	
	-2.52	1.30	1.58	-2.75	
	-3.62	-0.23	0.23	-3.43	
water	graphite	graphite	graphite	graphite	water

(b) MCNP5 (Bousbia-Salah et al., 2008)

Fig. 16. Deviations (in %) of power distribution calculated by OpenMC and MCNP5 with respect to Serpent, per each fuel element. The different cases are ordered as indicated in Fig. 15.

external codes.

The Serpent results for unit cell k_{∞} calculations are consistently higher with respect to EPRI-CELL and WIMS-D4 results, with average differences of 490 and 280 pcm for HEU and LEU, respectively. These differences are not significant since the differences between EPRI-CELL and WIMS-D4 results range between 50 and 150 pcm.

A comparison of the Serpent generated few group cross section was performed against the ANL benchmark results. The comparison includes fission and absorption cross sections for ^{235}U and ^{238}U in three energy groups – fast, epithermal and thermal. The agreement is very good except for the fission cross section of ^{238}U , where the values calculated by Serpent for the epithermal group are significantly larger than the ones calculated by EPRI-CELL code. These

differences are most likely due to pronounced differences in neutron data libraries used by EPRI-CELL code (ENDF/B-IV) and Serpent (ENDF/B-VII.1).

The effect of the usage of ADFs in full core calculations is demonstrated in Table 5, where the differences in k_{eff} values between DYN3D and Serpent drop once ADFs are used. Moreover, the results of both Serpent and DYN3D are in an excellent agreement with one another, and in very good agreement with the results of other Monte Carlo codes, e.g. (Bousbia-Salah et al., 2008) and (Chaudri and Mirza, 2015).

The mid-plane radial flux distribution and the axial flux distribution in the flux trap are in very good agreement with the results in (IAEA, 1980) and in Bousbia-Salah et al. (2008); Chaudri and Mirza (2015). The power distributions calculated by Serpent for all cases show good agreement with the results obtained with MCNP5 and OpenMC with small relative errors of up to 5% per fuel element. Both MCNP5 and OpenMC exhibit higher peaking factors with respect to Serpent. On the other hand, the nodal diffusion code DYN3D exhibit lower peaking factors.

Finally, the capabilities of the Serpent/DYN3D code system to calculate an MTR research reactor were demonstrated and compared for steady state calculations. On-going and future work includes the coupling of the Serpent/DYN3D code system to a time dependent thermal-hydraulic system code, THERMO-T, which is being developed at Ben-Gurion University (Margulis and Gilad, 2015), for the purpose of accident analyses and asymmetric transient calculations in research reactors. For further characterization and establishment of our codes performances, we are currently engaged in benchmarking them against actual LOFA and RIA experimental measurements performed in the ETRR-2, IEA-R1, and SPERT-IV reactors. The newly developed system code THERMO-T is currently undergoing comprehensive comparisons to different codes in different accident scenarios available in the IAEA TECDOC 643 (IAEA, 1992) and the IAEA Technical Reports Series No. 480 (IAEA, 2015), which provide both numerical (code-to-code) and experimental data for reactivity insertion and loss of flow accidents for different types of reactors.

water	graphite	graphite	graphite	graphite	water
	4.62	-0.93	-0.93	4.48	
water	4.01	-1.13	-1.13	4.25	water
	3.83	0.96	1.00	4.01	
	3.86	-0.34	-0.34	3.62	
0.72	0.28	-2.13	-2.13	-0.33	-0.05
0.27	-0.28	-2.11	-1.89	-0.28	0.52
-0.22	-2.08	-1.85	-2.01	-1.74	-1.15
-0.17	0.90	-2.11	-2.11	0.09	0.08
-2.05	0.51	-2.87	water	-2.87	0.24
-1.71	0.56	-2.88		-2.88	0.02
0.48	-0.18	-2.88	water	-2.88	0.08
-1.91	0.45	-3.07		-2.70	0.72
0.47	-0.03	-1.91	-2.13	-0.33	0.22
0.76	0.02	-2.00	-2.22	-0.28	0.27
-0.33	-1.88	-1.72	-1.79	-1.74	-0.30
0.08	0.90	-1.88	-2.11	0.90	0.08
water	4.72	-0.93	-1.18	4.23	water
	4.24	-0.62	-0.87	4.24	
	3.87	0.99	1.16	3.78	
	3.86	-0.09	-0.09	3.62	
water	graphite	graphite	graphite	graphite	water

Fig. 17. Deviations (in %) of power distribution calculated by DYN3D with respect to Serpent, per each fuel element. The different cases are ordered as indicated in Fig. 15.

Appendix A. Comparison of atomic densities vs. burnup

Table A.1

Atom densities for HEU fuel vs. burnup – comparison between ANL EPRI-CELL (IAEA, 1980), WIMS-D4 (Bousbia-Salah et al., 2008) and Serpent (units in $10^{24} \times \text{cm}^{-3}$).

Depletion (%)	²³⁵ U			²³⁶ U		
	EPRI-CELL	WIMS-D4	Serpent	EPRI-CELL	WIMS-D4	Serpent
0	1.61790E-03	1.61790E-03	1.61790E-03	0.0	0.0	0.0
5	1.53701E-03	1.53702E-03	1.53701E-03	1.34683E-05	1.36535E-05	1.34880E-05
10	1.45612E-03	1.45612E-03	1.45611E-03	2.68848E-05	2.72623E-05	2.68756E-05
25	1.21342E-03	1.21342E-03	1.21343E-03	6.62984E-05	6.74525E-05	6.62609E-05
30	1.13254E-03	1.13253E-03	1.13253E-03	7.91391E-05	8.05315E-05	7.91249E-05
45	8.89845E-04	8.89840E-04	8.89845E-04	1.16718E-04	1.18999E-04	1.16857E-04
50	8.08949E-04	8.08948E-04	8.08950E-04	1.28901E-04	1.31486E-04	1.29122E-04
Depletion (%)	²³⁸ U			²³⁹ Pu		
	EPRI-CELL	WIMS-D4	Serpent	EPRI-CELL	WIMS-D4	Serpent
0	1.20200E-04	1.20200E-04	1.20200E-04	0.0	0.0	0.0
5	1.19729E-04	1.19754E-04	1.19752E-04	4.37692E-07	4.14728E-07	3.63887E-07
10	1.19231E-04	1.19282E-04	1.19289E-04	8.47746E-07	8.03823E-07	7.46947E-07
25	1.17684E-04	1.17757E-04	1.17868E-04	1.80022E-06	1.75804E-06	1.63092E-06
30	1.17146E-04	1.17251E-04	1.17376E-04	2.03037E-06	1.97171E-06	1.84876E-06
45	1.15456E-04	1.15574E-04	1.15839E-04	2.47988E-06	2.44499E-06	2.28441E-06
50	1.14857E-04	1.15010E-04	1.15297E-04	2.55349E-06	2.50090E-06	2.36462E-06
Depletion (%)	¹³⁵ Xe			¹⁴⁹ Sm		
	EPRI-CELL	WIMS-D4	Serpent	EPRI-CELL	WIMS-D4	Serpent
0	0.0	0.0	0.0	0.0	0.0	0.0
5	1.70943E-08	1.62895E-08	1.62985E-08	1.33927E-07	1.39595E-07	1.28956E-07
10	1.64155E-08	1.56175E-08	1.55178E-08	1.28239E-07	1.41498E-07	1.27905E-07
25	1.40338E-08	1.31289E-08	1.31939E-08	1.07554E-07	1.37449E-07	1.18103E-07
30	1.32194E-08	1.24824E-08	1.24070E-08	1.00694E-07	1.35540E-07	1.14112E-07
45	1.07091E-08	9.90483E-09	9.97726E-09	8.01311E-08	1.24911E-07	1.00097E-07
50	9.84972E-09	9.17715E-09	9.14159E-09	7.32815E-08	1.17549E-07	9.47061E-08

Table A.2

Atom densities for LEU fuel vs. burnup – comparison between ANL EPRI-CELL (IAEA, 1980), WIMS-D4 (Bousbia-Salah et al., 2008) and Serpent (units in $10^{24} \times \text{cm}^{-3}$).

Depletion (%)	²³⁵ U			²³⁶ U		
	EPRI-CELL	WIMS-D4	Serpent	EPRI-CELL	WIMS-D4	Serpent
0	2.25360E-03	2.25360E-03	2.25360E-03	0.0	0.0	0.0
5	2.14092E-03	2.14092E-03	2.14092E-03	1.94582E-05	1.97571E-05	1.95176E-05
10	2.02823E-03	2.02824E-03	2.02824E-03	3.88442E-05	3.94491E-05	3.88695E-05
25	1.69020E-03	1.69018E-03	1.69020E-03	9.56508E-05	9.74379E-05	9.57033E-05
30	1.57752E-03	1.57752E-03	1.57752E-03	1.14100E-04	1.16255E-04	1.14192E-04
45	1.23952E-03	1.23949E-03	1.23948E-03	1.67779E-04	1.71363E-04	1.68209E-04
50	1.12691E-03	1.12688E-03	1.12680E-03	1.85044E-04	1.89175E-04	1.85696E-04
Depletion (%)	²³⁸ U			²³⁹ Pu		
	EPRI-CELL	WIMS-D4	Serpent	EPRI-CELL	WIMS-D4	Serpent
0	8.90050E-03	8.90050E-03	8.90050E-03	0.0	0.0	0.0
5	8.88775E-03	8.88776E-03	8.88732E-03	1.13740E-05	1.13074E-05	1.06550E-05
10	8.87411E-03	8.87415E-03	8.87363E-03	2.20424E-05	2.19337E-05	2.14239E-05
25	8.83036E-03	8.82938E-03	8.82968E-03	4.74782E-05	4.81672E-05	4.72354E-05
30	8.81469E-03	8.81378E-03	8.81391E-03	5.39063E-05	5.45263E-05	5.37287E-05
45	8.76349E-03	8.76100E-03	8.76213E-03	6.75486E-05	6.91062E-05	6.77308E-05
50	8.74467E-03	8.74231E-03	8.74306E-03	7.03139E-05	7.16456E-05	7.07073E-05
Depletion (%)	¹³⁵ Xe			¹⁴⁹ Sm		
	EPRI-CELL	WIMS-D4	Serpent	EPRI-CELL	WIMS-D4	Serpent
0	0.0	0.0	0.0	0.0	0.0	0.0
5	2.30226E-08	2.21224E-08	2.22400E-08	1.91678E-07	2.01798E-07	1.87893E-07
10	2.24095E-08	2.15200E-08	2.14778E-08	1.86339E-07	2.08996E-07	1.89025E-07
25	1.98787E-08	1.87846E-08	1.90361E-08	1.61934E-07	2.15206E-07	1.81357E-07
30	1.89700E-08	1.81255E-08	1.81527E-08	1.53457E-07	2.11683E-07	1.77086E-07
40	1.60514E-08	1.50798E-08	1.52551E-08	1.27167E-07	2.01752E-07	1.61065E-07
50	1.50123E-08	1.42346E-08	1.42484E-08	1.18131E-07	1.91742E-07	1.54308E-07

Appendix B. Comparison of k_{∞} vs. burnup

Table B.1

Unit cell infinite multiplication factor k_{∞} HEU and LEU fuel vs. burnup – comparison between ANL EPRI-CELL (IAEA, 1980), WIMS-D4 (Bousbia-Salah et al., 2008) and Serpent.

Depletion (%)	HEU (93 wt.%)			LEU (20 wt.%)		
	EPRI-CELL	WIMS-D4	Serpent ^a	EPRI-CELL	WIMS-D4	Serpent ^a
0	1.73698	1.73545	1.74893	1.65475	1.65207	1.66223
5	1.63697	1.63751	1.64907	1.56410	1.56317	1.57101
10	1.61653	1.61576	1.62822	1.54447	1.54258	1.55090
25	1.54853	1.54619	1.55914	1.47972	1.47721	1.48459
30	1.52227	1.51902	1.53269	1.45544	1.45237	1.45999
45	1.42692	1.42401	1.43651	1.37191	1.37057	1.37543
50	1.38761	1.38474	1.39696	1.33935	1.33815	1.34308

^a The statistical uncertainty is less than 7 pcm for all simulations.

References

- Abdelrazek, I.D., Abo-Elmour, A.G., Gaheen, M.A., 2015. Thermal hydraulic analysis of ETRR-2 using RELAP5 code. *Kerntechnik* 80 (1), 32–39.
- Adorni, M., Bousbia-salah, A., D'Auria, F., Hamidouche, T., 2006. Application of best estimate thermalhydraulic codes for the safety analysis of research reactors. In: International Conference on Nuclear Energy for New Europe 2006.
- Adorni, M., Bousbia-salah, A., D'Auria, F., Hamidouche, T., 2007. Accident analysis in research reactors. In: International Conference on Nuclear Energy for New Europe 2007.
- Adorni, M., Bousbia-Salah, A., Hamidouche, T., Maro, B.D., Pierro, F., D'Auria, F., 2005. Analysis of partial and total flow blockage of a single fuel assembly of an {MTR} research reactor core. *Ann. Nucl. Energy* 32 (15), 1679–1692. <http://www.sciencedirect.com/science/article/pii/S0306454905001337>.
- Arshi, S.S., Khalafi, H., Mirvakili, S., 2015. Preliminary thermal-hydraulic safety analysis of tehran research reactor during fuel irradiation experiment. *Prog. Nucl. Energy* 79 (0), 32–39. <http://www.sciencedirect.com/science/article/pii/S014919701400273X>.
- Azzoune, M., Mammou, L., Boulheouchat, M., Zidi, T., Mokeddem, M., Belaid, S., Salah, A.B., Meftah, B., Boumediene, A., 2010. NUR research reactor safety analysis study for long time natural convection (NC) operation mode. *Nucl. Eng. Des.* 240 (4), 823–831. <http://www.sciencedirect.com/science/article/pii/S0029549309006335>.
- Bousbia-Salah, A., Benkharfia, H., Kriangchaiporn, N., Petrucci, A., D'Auria, F., Ghazi, N., 2008. MTR benchmark static calculations with MCNP5 code. *Ann. Nucl. Energy* 35 (5), 845–855. <http://www.sciencedirect.com/science/article/pii/S0306454907002617>.
- Bousbia-Salah, A., D'Auria, F., 2007. Use of coupled code technique for best estimate safety analysis of nuclear power plants. *Prog. Nucl. Energy* 49 (1), 1–13. <http://www.sciencedirect.com/science/article/pii/S0149197006001077>.
- Bretschler, M., Hanan, N., Matos, J., October 1999. Neutronic safety parameters and transient analyses for Poland's MARIA research reactor. In: Abstracts and Papers of the 1999 International RERTR Meeting. Argonne National Laboratory.
- Brown, F.B., 2006. On the use of Shannon entropy of the fission distribution for assessing convergence of Monte Carlo criticality calculations. In: Proceedings of PHYSOR-2006 American Nuclear Society Topical Meeting on Reactor Physics, Organized and Hosted by the Canadian Nuclear Society. Vancouver, BC, Canada. 2006 September 10–14.
- Chatzidakis, S., Hainoun, A., Doval, A., Alhabet, F., Francioni, F., Ikonopoulou, A., Ridikas, D., 2014. A comparative assessment of independent thermal-hydraulic models for research reactors: the RSG-GAS case. *Nucl. Eng. Des.* 268 (0), 77–86. <http://www.sciencedirect.com/science/article/pii/S0029549313007000>.
- Chatzidakis, S., Ikonopoulou, A., Day, S.E., 2012. PARET-ANL modeling of a SPERT IV experiment under different departure from nucleate boiling correlations. *Nucl. Technol.* 177 (1), 119–131.
- Chatzidakis, S., Ikonopoulou, A., Ridikas, D., 2013. Evaluation of RELAP5/MOD3 behavior against loss of flow experimental results from two research reactor facilities. *Nucl. Eng. Des.* 255, 321–329.
- Chaudri, K.S., Mirza, S.M., 2015. Burnup dependent Monte Carlo neutron physics calculations of IAEA MTR benchmark. *Prog. Nucl. Energy* 81 (0), 43–52. <http://www.sciencedirect.com/science/article/pii/S0149197015000037>.
- Costa, A.L., Reis, P.A.L., Silva, C.A.M., Pereira, C., Veloso, M.A.F., Guerra, B.T., Soares, H.V., Mesquita, A.Z., 2011. Nuclear Power - System Simulations and Operation. InTech, Ch. 2. Safety Studies and General Simulations of Research Reactors Using Nuclear Codes, pp. 21–42. <http://www.intechopen.com/books/nuclear-power-system-simulations-and-operation/safety-studies-and-general-simulations-of-research-reactors-using-nuclear-codes>.
- D'Auria, F., Bousbia-Salah, A., 2006. Accident analysis in research reactors. In: Book of Abstracts 15th Pacific Basin Nuclear Conference. Australian Nuclear Association, p. 331.
- D'Auria, F., Bousbia-salah, A., Petrucci, A., Nevo, A.D., February 2006. State of the art in using best estimate calculation tools in nuclear technology. *Nucl. Eng. Technol.* 38 (1), 11–32.
- Deen, J.R., Hanan, N.A., Smith, R.S., Matos, J.E., Egorenkov, P.M., Nasonov, V.A., October 1999. Neutronic safety parameters and transient analyses for potential LEU conversion of the IR-8 research reactor. In: Abstracts and Papers of the 1999 International RERTR Meeting. Argonne National Laboratory and Russian Research Centre Kurchatov Institute.
- Fridman, E., Leppanen, J., 2012. Revised methods for few-group cross sections generation in the serpent Monte Carlo code. In: PHYSOR 2012 Advances in Reactor Physics Linking Research, Industry, and Education Knoxville, Tennessee, USA, April 15–20, 2012. American Nuclear Society, LaGrange Park, IL.
- Fridman, E., Leppanen, J., Wemple, C., 2013. Comparison of serpent and HELIOS-2 as applied for the PWR few-group cross section generation. In: International Conference on Mathematics and Computational Methods Applied to Nuclear Science & Engineering (M&C 2013), Sun Valley, Idaho, USA, May 5–9, 2013.
- Grundmann, U., Rohde, U., Mittag, S., 2000. DYN3D – three-dimensional core model for steady state and transient analysis of thermal reactors. In: PHYSOR 2000-Advances in Reactor Physics and Mathematics and Computation into the Next Millennium, Pittsburgh, PA, USA.
- Grundmann, U., Rohde, U., Mittag, S., 2005. DYN3D Version 3.2 Code for Calculation of Transients in Light Water Reactors (LWR) with Hexagonal or Quadratic Fuel Elements Description of Models and Methods. Tech. Rep. FZR-434. Helmholtz-Zentrum Dresden-Rossendorf (HZDR), Dresden, Germany.
- Hainoun, A., Doval, A., Umbehaun, P., Chatzidakis, S., Ghazi, N., Park, S., Mladin, M., Shokr, A., 2014. International benchmark study of advanced thermal hydraulic safety analysis codes against measurements on IAEA-R1 research reactor. *Nucl. Eng. Des.* 280 (0), 233–250. <http://www.sciencedirect.com/science/article/pii/S0029549314004269>.
- Hainoun, A., Schaffrath, A., 2001. Simulation of subcooled flow instability for high flux research reactors using the extended code ATHLET. *Nucl. Eng. Des.* 207 (2), 163–180. <http://www.sciencedirect.com/science/article/pii/S0029549300004106>.
- Hamidouche, T., Bousbia-Salah, A., 2010. Assessment of RELAP5 point kinetic model against reactivity insertion transient in the IAEA 10 MW MTR research reactor. *Nucl. Eng. Des.* 240 (3), 672–677. <http://www.sciencedirect.com/science/article/pii/S0029549309005597>.
- Hamidouche, T., Bousbia-Salah, A., Adorni, M., D'Auria, F., 2004. Dynamic calculations of the IAEA safety MTR research reactor benchmark problem using RELAP5/3.2 code. *Ann. Nucl. Energy* 31 (12), 1385–1402. <http://www.sciencedirect.com/science/article/pii/S0306454904000581>.
- Hamidouche, T., Bousbia-Salah, A., Si-Ahmed, E.K., D'Auria, F., 2008. Overview of accident analysis in nuclear research reactors. *Prog. Nucl. Energy* 50 (1), 7–14. <http://www.sciencedirect.com/science/article/pii/S0149197007002326>.
- Hamidouche, T., Bousbia-Salah, A., Si-Ahmed, E.K., Mokeddem, M.Y., D'Auria, F., 2009. Application of coupled code technique to a safety analysis of a standard MTR research reactor. *Nucl. Eng. Des.* 239 (10), 2104–2118. <http://www.sciencedirect.com/science/article/pii/S0029549309000274X>.
- Hari, S., Hassan, Y.A., Tu, J., 2000. Analysis of transient events without scram in a research reactor using the RELAP5/MOD3.2 computer code. *Nucl. Technol.* 130 (3), 296–309.
- Hedayat, A., Davilu, H., Jafari, J., 2007. Loss of coolant accident analyses on tehran research reactor by RELAP5/MOD3.2 code. *Prog. Nucl. Energy* 49 (7), 511–528. <http://www.sciencedirect.com/science/article/pii/S0149197007000704>.
- Housiadas, C., 2000. Simulation of loss-of-flow transients in research reactors. *Ann. Nucl. Energy* 27 (18), 1683–1693. <http://www.sciencedirect.com/science/article/pii/S0306454900000530>.
- IAEA, 1980. Research Reactor Core Conversion from the Use of High-enriched Uranium to the Use of Low Enriched Uranium Fuels Guidebook. TECDOC 233. IAEA.
- IAEA, 1992. Research Reactor Core Conversion Guidebook. TECDOC 643. IAEA.
- IAEA, 2007. Use and Development of Coupled Computer Codes for the Analysis of Accidents at Nuclear Power Plants. Tech. rep. International Atomic Energy Agency.
- IAEA, 2008. Innovative methods in research reactor analysis: benchmark against

- experimental data on neutronics and thermalhydraulic computational methods and tools for operation and safety analysis of research reactors. In: Meeting Report of the 1st Research Coordination Meeting of the CRP No. 1496, Vienna, Austria.
- IAEA, 2010. Innovative methods in research reactor analysis: benchmark against experimental data on neutronics and thermalhydraulic computational methods and tools for operation and safety analysis of research reactors. In: Meeting Report of the 2nd Research Coordination Meeting of the CRP No. 1496, Vienna, Austria.
- IAEA, 2011. Innovative methods in research reactor analysis: benchmark against experimental data on neutronics and thermalhydraulic computational methods and tools for operation and safety analysis of research reactors. In: Meeting report of the 3rd Research Coordination Meeting of the CRP No. 1496, Aix-en-Provence, France.
- IAEA, 2012. Innovative methods in research reactor analysis: benchmark against experimental data on neutronics and thermalhydraulic computational methods and tools for operation and safety analysis of research reactors. In: Meeting Report of the 4th Research Coordination Meeting of the CRP No. 1496, Vienna, Austria.
- IAEA, 2015. Technical Reports Series No. 480: Research Reactor Benchmarking Database: Facility Specification and Experimental Data. Tech. rep.. IAEA.
- Khan, S.U.-D., Khan, S.U.-D., Peng, M., 2014. Flow blockage accident or loss of flow accident by using comparative approach of NK/TH coupling codes and RELAP5 code. *Ann. Nucl. Energy* 64 (0), 311–319. <http://www.sciencedirect.com/science/article/pii/S0306454913005409>.
- Leppanen, J., 2007. Development of a New Monte Carlo Reactor Physics Code. Ph.D. thesis. Helsinki University of Technology.
- Leppanen, J., Pusa, M., Viitanen, T., Valtavirta, V., Kaltiaisenaho, T., 2015. The serpent Monte Carlo code: status, development and applications in 2013. *Ann. Nucl. Energy* 82 (0), 142–150. <http://www.sciencedirect.com/science/article/pii/S0306454914004095>.
- Lu, Q., Qiu, S., Su, G., 2009. Flow blockage analysis of a channel in a typical material test reactor core. *Nucl. Eng. Des.* 239 (1), 45–50. <http://www.sciencedirect.com/science/article/pii/S0029549308002884>.
- Margulis, M., Gilad, E., 2015. Analysis of protected RIA and LOFA in plate type research reactor using coupled neutronics thermal-hydraulics system code. In: The 16th International Topical Meeting on Nuclear Reactor Thermal Hydraulics (NURETH-16), Chicago, Illinois, August 30–September 4, 2015.
- Omar, H., Ghazi, N., Alhabit, F., Hainoun, A., 2010. Thermal hydraulic analysis of syrian MNSR research reactor using RELAP5/Mod3.2 code. *Ann. Nucl. Energy* 37 (4), 572–581. <http://www.sciencedirect.com/science/article/pii/S0306454909003958>.
- Pusa, M., 2013. Numerical Methods for Nuclear Fuel Burnup Calculations. Ph.D. thesis. Aalto University, Finland.
- Reis, P.A., Costa, A.L., Pereira, C., Veloso, M.A., Mesquita, A.Z., Soares, H.V., de P. Barros, G., 2010. Assessment of a RELAP5 model for the IPR-R1 TRIGA research reactor. *Ann. Nucl. Energy* 37 (10), 1341–1350. <http://www.sciencedirect.com/science/article/pii/S0306454910001842>.
- Soares, H.V., Aronne, I.D., Costa, A.L., Pereira, C., Veloso, M.A.F., 2014. Analysis of loss of flow events on brazilian multipurpose reactor using the RELAP5 code. *Int. J. Nucl. Energy* 2014, 186189. <http://dx.doi.org/10.1155/2014/186189>.
- Woodruff, W., Hanan, N., Matos, J., 1997. A comparison of the RELAP5/MOD3 and PARET/ANL codes with the experimental transient data from the SPERT IV D-12/25 series. In: Proceedings of the International Meeting on Reduced Enrichment for Research and Test Reactors, October 5–10, Wyoming, USA.
- Woodruff, W., Hanan, N., Smith, R., Matos, J., 1996. A comparison of the PARET/ANL and RELAP5/MOD3 codes for the analysis of IAEA benchmark transients. In: Proceedings of the International Meeting on Reduced Enrichment for Research and Test Reactors, October 7–10. Argonne National Laboratory, Seoul, Republic of Korea, p. 233.

Glossary

- 3D**: Three dimensional. 1, 4
- ADF**: Assembly Discontinuity Factor. 1, 8
- ANL**: Argon National Laboratory. 1
- BOL**: Beginning Of Life. 1, 5
- CPU**: Computing Processing Unit. 1, 4
- DF**: Discontinuity Factor. 1
- EOL**: End Of Life. 1, 5
- HET**: Heterogeneous. 1
- HEU**: Highly Enriched Uranium. 1, 3
- HOM**: Homogeneous. 1
- HZDR**: Helmholtz-Zentrum Dresden-Russendorf. 1
- IAEA**: International Atomic Energy Agency. 1, 3
- LEU**: Low Enriched Uranium. 1, 3
- MC**: Monte Carlo. 1
- MTR**: Material Test Reactor. 1, 3
- NK**: Neutron Kinetics. 1, 3
- NPP**: Nuclear Power Plant. 1, 3
- PC**: Predictor–Corrector. 1, 4
- RR**: Research Reactor. 1, 3
- TH**: Thermal-Hydraulics. 1, 3